RSC Advances

PAPER

View Article Online
View Journal | View Issue

Cite this: *RSC Adv.*, 2023, **13**, 11201

Modified carbon paste ion selective electrode for determining Cr(III) ions in aqueous solutions and some real samples using tetragonal zirconia nanoparticles†

Omar A. Fouad, *[a] Mohamed M. S. Wahsh,[b] Gehad G. Mohamed,[ac] Maher M. I. El Dessouky[a] and Maysa R. Mostafa[a]

Tetragonal zirconia (t-ZrO_2) nanoparticles (ionophore) are used in newly designed and improved ion selective electrodes for chromium ion detection as an alternative, low-cost, high-precision, and selectivity method. Tetragonal zirconia nanoparticles were synthesized using a modified co-precipitation technique and calcined at 1000 °C for an hour. The phase composition, surface area, microstructure, pore size and particle size of synthesized t-ZrO_2 nanoparticles were examined using the X-ray diffraction (XRD), Brunauer–Emmett–Teller (BET), transmission electron microscope (TEM) and scanning electron microscopy (SEM) attached with an EDAX unit, respectively. Results from XRD showed that the t-zirconia was synthesized and have nanocrystallites size about 20.2 nm. The nano size of t-ZrO_2 was confirmed by the SEM and TEM (the particle size between 26.48 and 40.4 nm), the mesoporous character (average pore size about 4.868 nm) and large surface area (76.2802 m^2 g^{-1}) was confirmed by BET analysis. The paste composition with 67.3 : 30.5 : 2.7 (wt%) graphite, t-ZrO_2, and TCP, respectively, exhibited the best results. With a detection limit of 1.0×10^{-8} mol L^{-1}, the electrode displayed a good Nernstian slope of 19.50 ± 0.10 mV $decade^{-1}$ over the concentration range from 1.0×10^{-2} to 1.0×10^{-8} mol L^{-1} of Cr(III) ions. The built-in sensor displayed a quick response time (7 s), was highly thermally stable in the range of 10 to 60 °C without departing from Nernstian behaviour and could be used for about 60 days in the pH range of 2.0 to 6.0. The electrode demonstrated excellent selectivity for the Cr(III) ion towards a variety of metal ions. For chromium ion determination, numerous spiked real samples, including honey, water, tea, coffee, milk, cheese, and cosmetics, were used. Validation methods were used, and the results showed that there is no significant difference between the two methods (ICP and ISE) at a 95% confidence level. In several real water samples, the estimated limits of detection, limits of quantification, percent recovery, standard deviation, and relative standard deviation showed the effectiveness of the proposed electrode in the potentiometric detection of Cr(III) ions.

Received 9th March 2023
Accepted 3rd April 2023

DOI: 10.1039/d3ra01563g

rsc.li/rsc-advances

1. Introduction

Chromium is applied to synthesize a variety of alloys like stainless steel and is also used to harden steel. Additionally, plastics can be chrome plated. Most leather is tanned with chromium. Chromium compounds are utilized as industrial catalysts and pigments (green, yellow, red, and orange colors). It also serves an important biological function by assisting in the utilization of glucose, a nutrient needed by all cells,[1] it also performs a crucial metabolic function. In water-based solutions, the established oxidation states of chromium in aqueous solutions are Cr(III) and Cr(VI). Compared to Cr(VI) compounds, Cr(III) is thought to be less hazardous.[2–4] But when taken in excess, about 1 mg daily, it is harmful.[5,6]

Alternative techniques, particularly spectrophotometry,[7] isotope dilution mass spectrometry,[8] cloud point extraction and flame atomic absorption spectrometry,[9] HPLC,[10] chromatography[10] inductively coupled plasma mass spectrometry,[11] have been considered for the monitoring of Cr(III) ions. Even though these techniques produced accurate, selective, and sensitive results, they are hindered by expensive, specialized gear besides laborious and time-consuming sample preparation. However, electrochemical techniques, which are safe for the environment, have the benefits of high sensitivity, simplicity of use, and

[a]*Chemistry Department, Faculty of Science, Cairo University, 12613 Giza, Egypt. E-mail: oahmed@sci.cu.edu.eg*

[b]*Refractories, Ceramics and Building Materials Department, National Research Centre, 12622, Cairo, Egypt*

[c]*Nanoscience Department, Basic and Applied Sciences Institute, Egypt-Japan University of Science and Technology, New Borg El Arab, Alexandria, 21934, Egypt*

† Electronic supplementary information (ESI) available. See DOI: https://doi.org/10.1039/d3ra01563g

mobility.[4,12] Ion concentrations in various substances can now be directly determined potentiometrically using ion-selective electrodes (ISEs).[4,13–16]

One of the extremely important ISE is modified carbon paste-based sensors (MCPEs) which formed from blending of pasting liquid (plasticizer), conductive graphite powder and ion carrier and offer a lot of merits include being simple to apply to colored and turbid liquids, affordable, providing satisfactory selectivity, having a minimal detection limit, possessing outstanding accuracy, and offering a wide concentration range. The ion carrier employed in the MCPE determines all of these benefits.[17–19] Due to their great repeatability, ability to be altered by a span of modifiers, and usage of less expensive materials, they have been favored as sensing materials and are frequently employed for voltametric measurements.[20,21]

Nanoparticles exhibiting conduction sites for electron transfer, for instance oxide NPs, semiconductor NPs, metal NPs, and even composite NPs, are extensively utilized in electrochemical sensors.[22] One of the most significant nanoparticles is zirconium oxide, sometimes denoted to as zirconia, is a white, crystalline solid utilized in coatings, ceramics, electronics, pigments, and some medical applications. It has exceptional mechanical characteristics and is very resistant to mechanical stress and cracking. ZrO_2 was well recognized for having a great resistance to heat as well as a thermal expansion coefficient of 1.08×10^{-5} K^{-1} and a melting point of 2700 °C. Because it doesn't absorb neutrons, is superconductive at low temperatures, and be able to employed to create superconducting magnets, zirconium is ideal for use in nuclear power plants.[23] It is non-reactive and chemically inert.[24]

At standard pressure and ambient temperature (STP), pure zirconia occurs as a monoclinic (m-ZrO_2) phase that changes into a tetragonal (t-ZrO_2) phase at about 1170 °C, a cubic fluorite structure (c-ZrO_2) at about 2370 °C.[25,26] The structure of pure ZrO_2 materials is significantly destroyed during the transition between the three ZrO_2 crystal forms, which is often associated by volume changes and shear strain.[26,27] Pure ZrO_2 is easily transformed throughout a heating–cooling cycle from the t-ZrO_2 phase to m-ZrO_2 phase, resulting in a volume shift that is primarily represented by a 5% volume expansion during cooling and a 3.25% volume shrinkage during heating.[28] Due to the breaking of its products and the buildup of tensile stress throughout pure ZrO_2 material, which generates a toughening effect, this significantly restricts the usage of pure ZrO_2 materials. As a result, pure ZrO_2 must be stabilized to generate the tetragonal and/or cubic phases, which give material has outstanding mechanical, thermal, and electrical properties.[25,26,28]

In an effort to control the structure of ZrO_2 materials and stop this t → m-ZrO_2 transformation, cations having a radii larger than those of Zr(IV) are incorporated into ZrO_2 lattices to replace part of the Zr(IV) lattice sites. At the same time, alternative solid solutions are developed in these ZrO_2 materials *via* systematic doping, that preserves the steady phase structure of the consequent doped ZrO_2 materials at ambient temperature and delivers a toughening impact for pure ZrO_2 materials.[26,29] Usually, the main components of doped stabilizers are alkaline earth and rare earth oxides. Ionic oxides and Zr(IV) should have radii that differ from one another by no more than 40%.[28,30] Especially noteworthy are the more often used MgO,[31] CaO,[32] Y_2O_3,[28,33] and CeO_2.[28,34] As a consequence of combining with these oxides, the m-ZrO_2 phase at ambient temperature prefers highly symmetric metastable structures (c and t-ZrO_2) that are comparable to those in pure zirconia but with dopant ions replaced on Zr(IV) positions and with a portion of oxygen positions unoccupied to preserve charge balance.[35,36] The crystal of ZrO_2 may be either fully or partially stabilized; however, fully stabilized zirconia (FSZ) (c-ZrO_2) has less advantageous mechanical properties than partially stabilized zirconia (PSZ), therefore the stabilizer concentrations should be lower than those required for full stabilization of ZrO_2.

Magnesium partially stabilized zirconia (Mg-PSZ) reveals high *R*-curve conduct owing to transference toughening, with a peak fracture toughness >20 $MPam^{1/2}$.[37,38] The stress-induced t → m-phase conversion is the fundamental mechanism. Through utilizing eutectoid and/or sub-eutectoid ageing process, along with an appropriate cooling rate, it is feasible to increase the quantity of reconfigurable tetragonal phase in Mg-PSZ and achieved desired fracture toughness.[37,38]

This work's objectives are to detail the synthesis of nano-t-ZrO_2, characterize it, integrate it within CPEs as a modifier, and measure its performance features for Cr(III) ion detection. Several characterization methods, such as powder X-ray diffraction (XRD), scanning electron microscopy (SEM) with EDAX, Transmission electron microscope (TEM) and Brunauer–Emmett–Teller (BET) analysis, were exploited to acquire comprehension of the structure and behaviors of the nano t-ZrO_2. For MCPE the impacts of t-ZrO_2-NPs concentration, plasticizer, pH, temperature, selectivity, and longevity were comprehensively evaluated. Both pure Cr(III) and several authentic samples could be detected using the MCPE as potentiometric sensors. The criteria for approach validity were looked at.

2. Experimental

2.1. Materials and methods

In every experiment, analytical reagent grade chemicals and reagents were employed, along with double distilled water. Sigma-Aldrich Chemie GmbH provided the zirconyl chloride octahydrate (purity 98%) and magnesium chloride hexahydrate (purity 99%) used in this study. Ammonia solution came from Riedel-deHaen in Germany, and Acros Organics in the USA provided the chromium chloride hexahydrate. Whereas dioctyl phthalate (DOP) and dibutyl phthalate (DBP) were provided by BHD, and *o*-nitrophenyloctylether (*o*-NPOE) was supplied by Fluka. Aldrich provided the tricresylphosphate (TCP) and graphite powder (1–2 μm). Ascorbic acid, $CoCl_2 \cdot 6H_2O$, $PbNO_3$, $NiCl_2 \cdot 6H_2O$, $AgNO_3$, NaCl, $CuCl_2 \cdot 2H_2O$, $MnCl_2 \cdot 4H_2O$ and varied metals chlorides like Fe(III), Mg(II), Ca(II), Co(II) and Ba(II) obtained from El-Nasr Company (Egypt) were utilized as interfering materials in the analytical category. All apparatus used are discussed in our previous studies.[4,12]

2.2. Synthesis of t-ZrO_2 nanoparticles

Using a modified co-precipitation process, the t-ZrO_2 nanoparticles were created. Using distilled water as a solvent, zirconyl chloride octahydrate solution (1 M) was created. The zirconyl chloride octahydrate solutions were then mixed with the magnesium chloride hexahydrate solutions in a quantity, corresponding to MgO weight percentage of 14. This ratio has been chosen to be consistent with the earlier studies that indicate pure t-ZrO_2 is present when the weight percentage of MgO is equal to 14, and less than this ratio the polyphase (monoclinic, tetragonal and cubic phases) ZrO_2 is frequently detected.[39] To stimulate a homogenous solution, the prepared solutions were blended with steady stirring for one hour. The Zr(IV) and Mg(II) chloride solutions were treated with ammonia dropwise until the pH was 10.5. This resulted in the preparation of Zr(IV) and Mg(II) hydroxides. The metal ions solutions were filtered through ashless filter paper (Whatman® Grade 41, England) to separate the precipitates, and the chloride ions were then eliminated by washing the mixture three times with distilled water. The precipitates have been initially dried for twenty-four hours at 90 °C, then calcined for 1 hour at 1000 °C with a 5 °C min^{-1} heating rate. Characterization of the synthesized pure t-ZrO_2 NPs have been acquired using X-ray diffraction, a scanning electron microscope (SEM) connected to an EDAX unit, transmission electron microscope (TEM) and Brunauer–Emmett–Teller (BET) analysis.

2.3. MCPE preparation

The black paste is homogeneously ground with 0.250 g, (5, 10, 15) mg, and 0.12 g of graphite powder, t-ZrO_2-NPs, and plasticizer, respectively, which are mixed in a mortar and pestle. The mixture was gently stuffed into the electrode's tube over one side then left there for 24 hours in distilled water to obstruct air intrusion. A fine tissue was utilized to sweep the graphite paste's surface prior to the test.

Calibration was carried out by measuring the potential of 1.0×10^{-10}–1.0×10^{-2} mol L^{-1} of Cr(III) solution starting from low to high concentration by transferring 5 mL aliquots of Cr(III) into 25 mL beakers at 25 °C (pH = 4) followed by immersing the CPE in conjunction with Ag/AgCl electrode in the solution. The potential change was plotted against the logarithm of Cr(III) ion.

2.4. Preparation of samples for the analysis

2.4.1. Milk and cheese samples. The cheese sample was processed handmade cheese that is commonly offered in local markets and is fashioned by adding vinegar to milk after boiling. A sample of milk was imported from an Egyptian market. After adding 50.0 mL of each specimen in 2 duplicates to an uncovered porcelain crucible that had previously been pretreated with 1 mL of strong nitric acid (65%), the crucible subsequently progressively heated over a hot plate (IKA, Tbilisi, Georgia) till fume terminated. For the cheeses, 10.0 g of every sample was inserted into two duplicate uncoated porcelain crucibles rinsed with 1 mL of pure nitric acid (65%) blended by deionized water (1 : 1) then left for fifteen min. Following that, both specimens have been ashed in a muffle furnace (Nabertherm, L15/11, Germany) that had been preheated to 250 °C and had been elevated in temperature progressively (by 50 °C after 30 min.) to 450 °C. Ashing was accomplished till grey ash was collected, the leftover subsequently dissolved in mild nitric acid, and the combination was progressively dried at 140 °C on a hot plate (IKA, Staufen, Germany). Samples were placed back into the muffle furnace after cooling for 30 minutes at 300 °C. Up till white ash was acquired, the stage before it was repeated. Finally, 5 mL of strong nitric acid was used to dissolve the ash samples, and that solution was then diluted to 25 mL (50 mL diluted for cheese samples). Two blank samples were performed using deionized water and filters in the same manner as when exploiting the reagents alone.[40]

2.4.2. Red tea sample. Five grams of tea were utilized to generate heating samples, which were subsequently filtered and completed in 50 mL of deionized water. The resultant solutions' pH was adjusted to be 5.[41] Mate tea was acquired from a Korean market, whereas red tea was purchased from an Egyptian store.

2.4.3. Coffee sample. Roasted and crushed coffee were placed in boiling water (95 to 100 °C), filtered, and then utilized to generate the coffee infuse. Afterward, 25 mL of the infuse that had been made by volume was condensed to produce around 2.5 mL of the final volume in a greenhouse with good ventilation and air interchange (Tecnal brand, TE-394/2 model, Piracicaba, SP, Brazil) at 60 °C. By soaking the crushed coffee sample with a 3 : 1 ratio of nitric and perchloric acids, the sample was mineralized.[42]

2.4.4. Cosmetics eye shadow sample. Each sample received 10 mL of digested acid (3 : 1 v/v HCl : HNO_3) after being pipetted into a digestion test tube with care at a weight of 0.5 g each sample. This was set for 30 minutes on the hot plate. Following digestion, the samples were brought up to a volume of 50 mL with distilled water, allowed to cool to ambient temperature, and then filtered.[43]

2.4.5. Honey sample. Each honey sample was weighed into 24 separate digestion tubes, each holding about 1 g. Then, using a measuring cylinder, about 10 mL of aqua regia were inserted to the digestion tubes containing the honey samples. To create a homogenous mixture, the aforementioned combination was gently shaken. The tubes holding the samples comprising aqua regia and honey were subsequently placed with digestion blocks on a hot plate. The setup hot plate's temperature was set to 100 °C. When the thermometer reached a temperature of 100 °C, the digestive tubes were put into the blocks. Sample solutions were heated for an hour, throughout which time they turned from deep yellow to pale yellow. Sample solutions that had been digested were then allowed to reach room temperature. Finally, a Whatman filter paper has been exploited to penetrate the solution. Distilled water was append to the digested sample solutions until they reached a final volume of 50 mL.[44]

3. Outcomes and interpretation

3.1. XRD for the prepared nano-t-ZrO_2

Fig. 1 exposes the XRD patterns of the prepared nano t-ZrO_2. Without any diffraction peaks corresponding to other phases, t-

ZrO_2 is the only significant phase that has been identified. According to the XRD pattern of pure t-ZrO_2, the sharp diffraction peaks at 30.27°, 35.22°, 42.92°, 50.50°, 60.25°, 62.97°, and 74.6° were attributed to the (0 1 1), (1 1 2), (0 1 1), (1 2 1), (0 2 2), and (2 2 0) planes, respectively. The $P4_2/nmc$ (137) space group, card number 2300612, and the tetragonal structure all suit these sharp peaks. So, in light of these XRD results, the pure t-ZrO_2 was successfully synthesized using 14 weight percent of MgO as a stabilizer. Additionally, the XRD pattern's existence of significant sharp peaks reveals that the synthesized nano t-ZrO_2 was crystalline and nanometric in scale. The average crystallite size of prepared nanoparticles is 20.2 nm (derived from the Debye–Scherrer equation).[4,45]

3.2. SEM in conjunction with EDAX of t-ZrO_2

The shape and microstructure of the surface of the prepared t-ZrO_2 nanoparticles were examined using scanning electron microscopy (SEM) in conjunction with EDAX, Digital Surf's Mountains Lab®, and Java 1.8.0172 with ImageJ (1.53e) software.[46,47] SEM images of the t-ZrO_2 nanoparticles showed their spherical-like shape, homogeneous matrix, smooth surface, and porous structure (Fig. (2A)). The SEM microphotographs also revealed the presence of different pore sizes and particles on the synthesized t-ZrO_2 nanoparticles.

The pores in the sample were seen to take on different colors using the color threshold method on SEM microphotographs with a 1 μm scale, as discovered in Fig. (2B). Using Digital Surf's Mountains Lab® program, it was determined that the overall percentage of pores and the average size of the pores were 13.54% and 39.68 nm, respectively.

Additionally, the Java 1.8.0172 with ImageJ (1.53e) tool was established to produce the Gaussian mixture model and histogram in Fig. (2C) to estimate the distribution of particle sizes. The average particle size of 40.4 nm was found for the t-ZrO_2 nanoparticles. The chemical composition of t-ZrO_2 nanoparticles was identified using EDAX data (Fig. (2D)). Magnesium constitutes about 1.8% of the composition, followed by zirconium (33.4%) and oxygen (64.8%). The EDAX dates exposed that the synthesized t-ZrO_2 nanoparticles sample had a homogenous distribution of all its constituent parts.

3.3. Transmission electron microscopy (TEM) of nano t-zirconia

The TEM was used to examine the morphology and particle sizes of the synthesized t-ZrO_2 nanoparticles. Fig. (3) demonstrates that the average particle size of the t-ZrO_2 NPs falls between 26.48 nm and 86.21 nm, which is in good consistency with the average crystallite size determined from XRD data (20.2 nm) and the average particle size determined from the SEM image analysis (40.4 nm). The outcome also supports the nanoscale synthesis of t-ZrO_2.

3.4. BET-analysis

The nitrogen adsorption (BET) measurements for t-ZrO_2 nanoparticles revealed a high surface area about 76.2802 $m^2\ g^{-1}$ with an average pore size about 4.868 nm and pore volume about 0.186 $cm^3\ g^{-1}$ which verified that the mesoporous structure of the nano t-ZrO_2.[12]

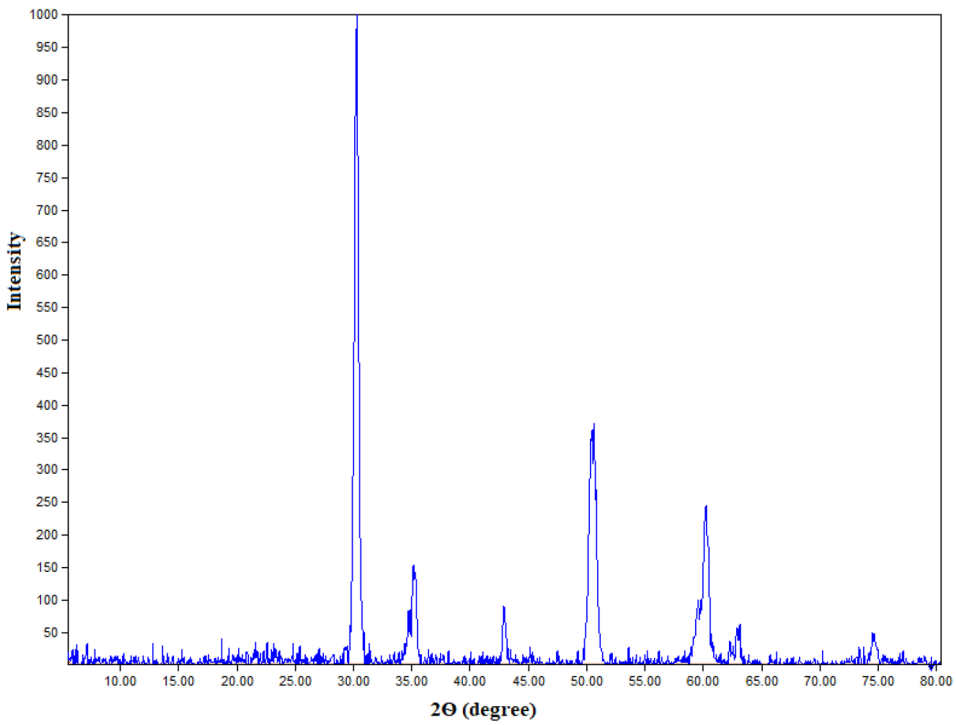

Fig. 1 XRD patterns of the t-ZrO_2 nanoparticles.

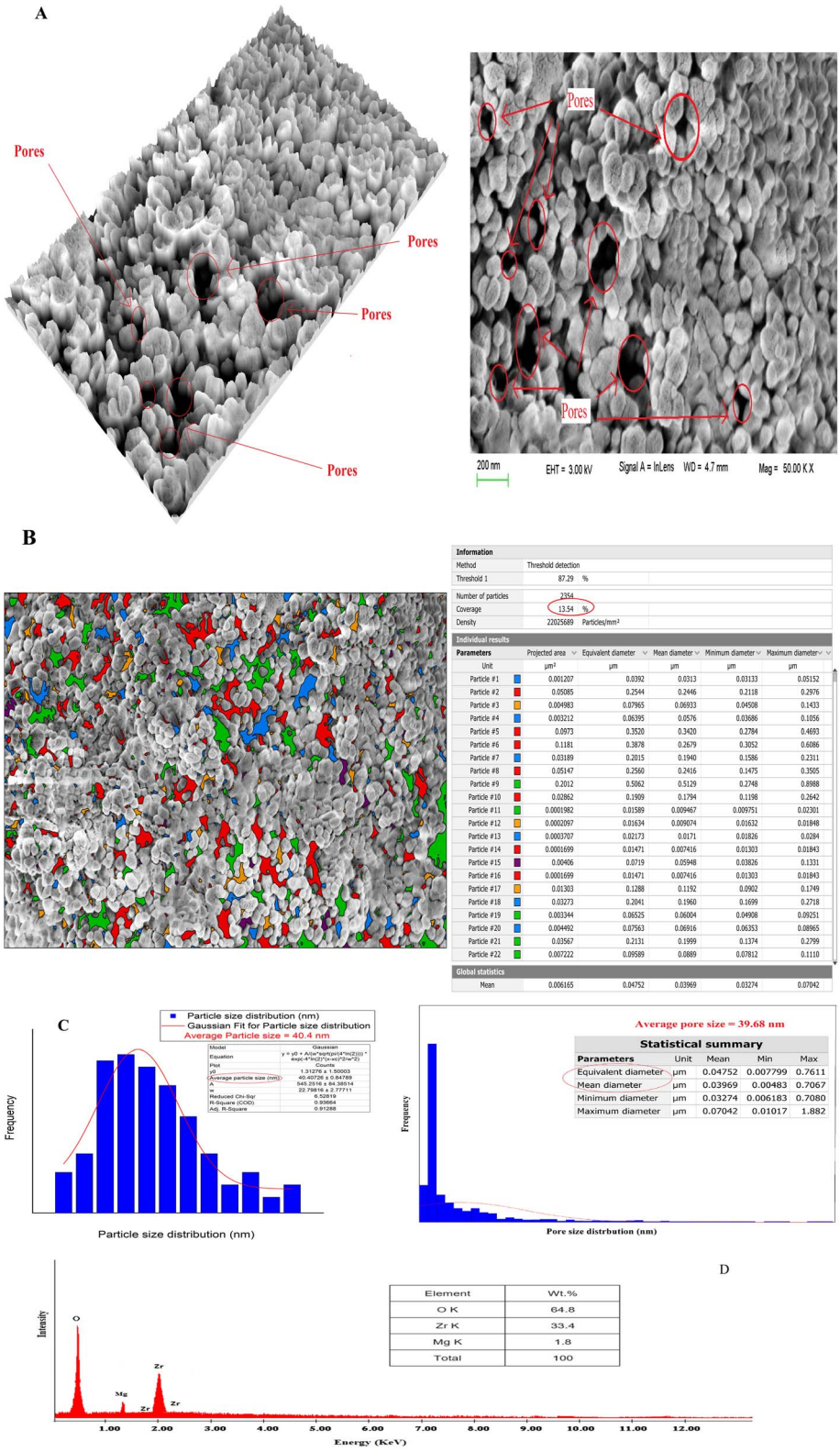

Fig. 2 The SEM microphotographs (A), particle and pore size distributions (B and C) and EDAX data (D) of the prepared t-ZrO_2 nanoparticles.

3.5. Electrochemical determination of Cr(III) ion with utilized electrodes

Many modified CPEs with nano t-zirconia as a powerful electroactive material, graphite sheets as a matrices and TCP as a solvent moderator have been synthesized to establish the best paste composition with the best effectiveness that complies to the Nernst equation.[16] In (ESI† Table S1) the outcomes are displayed. The calibration was performed by submerging the

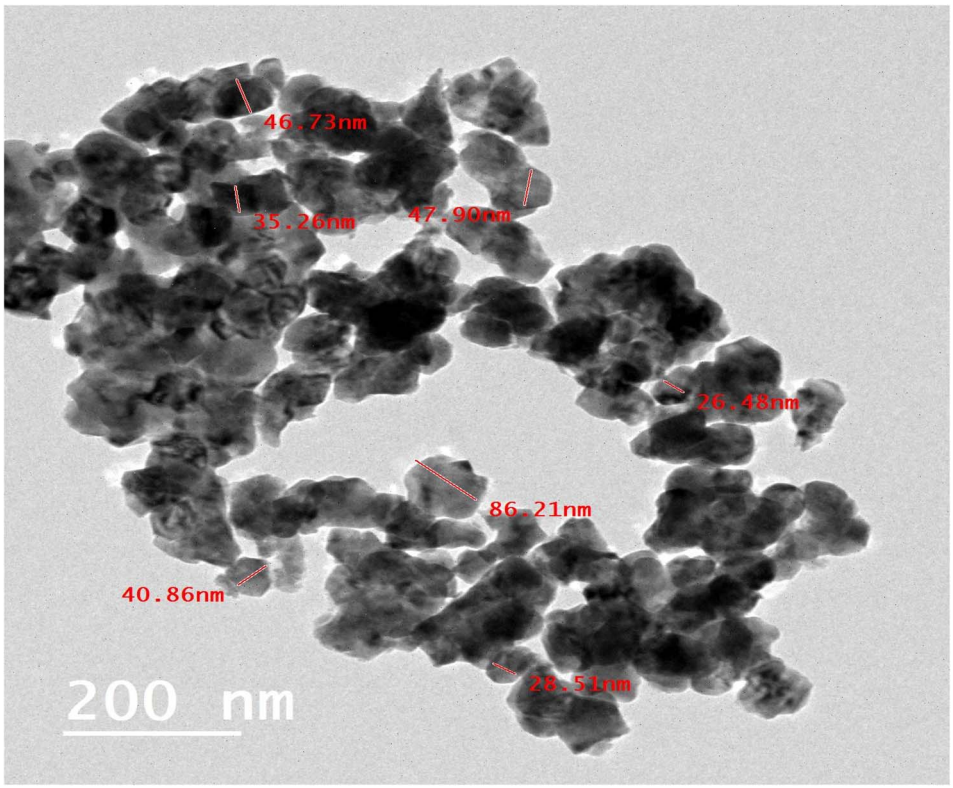

Fig. 3 The high-resolution TEM image (HR-TEM) of the prepared t-ZrO_2 nanoparticles.

electrodes associated with the double junction Ag/AgCl reference electrode in Cr(III) ion solutions with concentrations ranging from 1.0×10^{-8} to 1.0×10^{-2} mol L^{-1} which covers a wider range of concentrations than that reported in Barati *et al.*,[48] in which CPEs were evaluated throughout the interval from 1.0×10^{-3} to 1.0×10^{-6} mol L^{-1}.

Different modified CPEs were established with varied nano t-ZrO_2 contents, such as 5, 10, and 15 mg. Additionally, the effects of various plasticizers, such as DHP, DBP, TCP, DOP, and NPOE, were investigated. ESI† Tables (S1 and S2) pointed out the fact that the modified CPEs that had been treated with 10 mg of t-ZrO_2 and plasticized with TCP had the best Nernstian slope of 19.5 ± 0.10 mV decade^{-1}. The high *R*-square (0.998) is another evidence of the significance of the suggested model and the accuracy fit the model.

3.6. Surface analysis of the MCPE

In carbon paste electrodes, Fig. 4 (A and B), t-ZrO_2 nanoparticles (ionophores) are coupled with graphite sheets and TCP as a solvent moderator to increase the pores area of CPE to 19.88% of total measured area, which is higher than the pores area of t-ZrO_2 alone (13.54%), and to increase the average pore size to 1.359 nm with a range from 1.084 to 2.209 nm. Additionally, t-ZrO_2 nanoparticles can form a connection with the Cr(III)ion in real samples or pure solutions. This connection will alter the smoothness, roughen the electrode's surface, and cause the appearance of white spots as a consequence of the existence of Cr(III) ions on the surface of the electrode following soaking, as evidenced by the SEM image (Fig. (4C)).

Additionally, the Cr(III) ions existing in it and the quantitative data on the surface composition of the past both prior and following soaking in Cr(III) ion solution had also reinforced this mechanism, as seen in Fig. (4D). This result enhanced the CPE's porosity and selectivity for the Cr(III) ion. Therefore, it provides a capability for employing the suggested approach and the examined CPE for estimating the Cr(III) ion in either pure solution or real samples.

3.7. Effect of plasticizer

Plasticizers are believed to hold a substantial impact on how CPEs behave. Among increased ionic mobility and sensing material solubility, they also have decreased bulk resistance of the electrode as a result of their polarity properties. They strengthen the mechanical connections between the various electroactive carbon particles to establish a consistent, compact combination.[4,15,16] In accordance with the plasticization's lubricating hypothesis, the plasticizer molecules dispersed throughout the polymer and diminished the contacts (van der Waals forces). This enables the chains to pass each other speedily and leads to flexibility, softness, and elongation. It assumes that the plasticizer molecules are not permanently bound to the molecules but are free to self-associate. The non-polar section of the molecule must manage the polar section of the molecule so that it is not a powerful enough solvator to

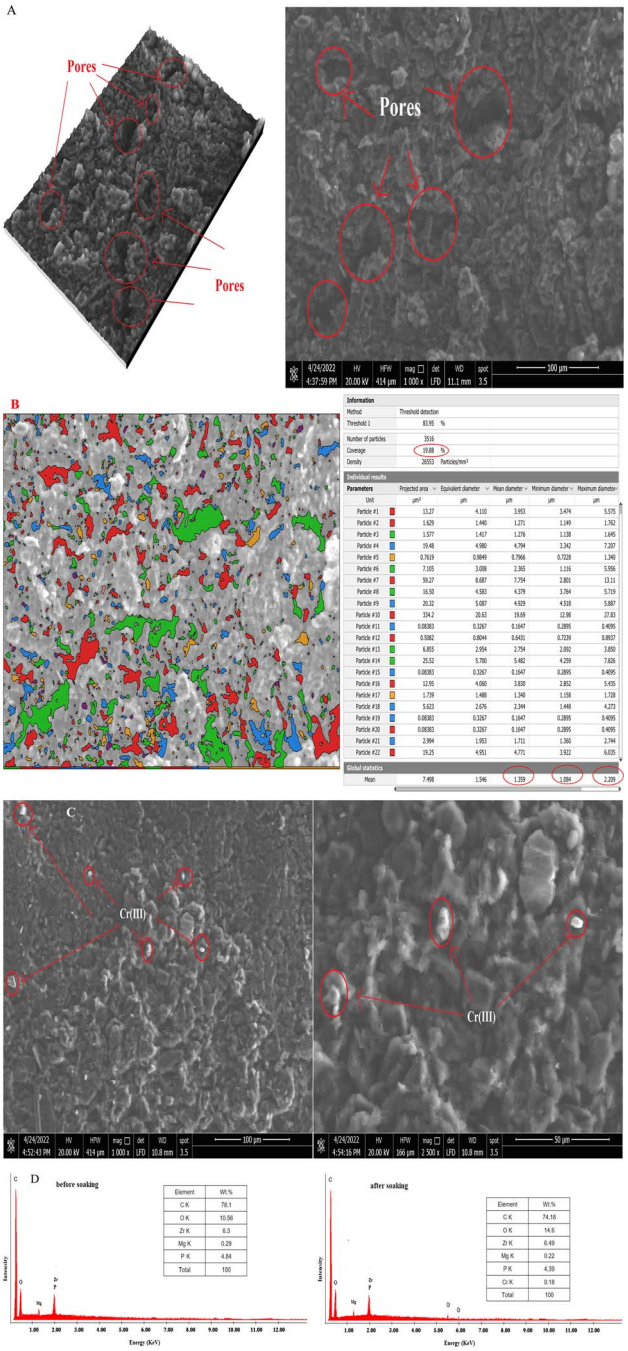

Fig. 4 (A and B) SEM picture with pores, (C) SEM image after soaking, and (D) EDAX analysis. Surface SEM and EDX examination of the suggested sensor surface (10 mg nano-t-ZrO_2 ionophore, 0.1 g TCP and 250 mg graphite).

disrupt the crystallinity of materials. To offer softening, the molecule's polar part must be capable of binding reversibly. Plasticizers merely exhibit a strong affinity; they do not assist in a chemical process that results in bonding or grafting.

According to prior studies,[4,12] the sensitivity and selectivity of ion-selective electrodes are known to be greatly influenced by the nature of the solvent mediator and any additives employed. Both the membrane's dielectric constant and the ionophore's mobility are influenced by the type of plasticizer. A plasticizer must have a variety of characteristics in order to be proper for use in sensors, according to Pérez *et al.*[49]. One or more of these features comprise a significant molecular weight, a low vapor pressure, and a large capacity to disintegrate the substrate and any additional additives existing in the matrix.

Five plasticizers with various polarities, including TCP, DBP, DHP, DOP, and *o*-NPOE plasticizers, were used to explore the impact of plasticizer type on the features of the researched sensor. It is realized that the electrode incorporating TCP frequently exhibits improved potentiometric responses, *i.e.*, sensitivity and linearity range of the calibration plots. Due to its significant dielectric constant and comparatively elevated molecular weight, it provides the best Nernstian slope (19.5 ± 0.10 mV decade^{-1}) if compared with the alternative plasticizers, whose slopes values were 48.01 ± 1.2, 30.40 ± 1.2, 32.50 ± 0.1, and 32.70 ± 0.2 mV decade^{-1} for DBP, DHP, DOP, and *o*-NPOE plasticizers, respectively.

3.8. The pH effect

By adding small volumes of HCl or/and NaOH (0.1–1 mol L^{-1} of each) and immersing the optimized electrode in 1.0 × 10^{-4} mol L^{-1} Cr(III) solution, the influence of pH on the effectiveness of the investigated electrode was studied over the pH range of 1–9. Also, the resulting potential of 1.0 × 10^{-6} mol L^{-1} of Cr(III) solution was recorded. Fig. (5) declares that the electrode has constant potential measurements (independent on the pH readings) in the pH range of 2.0–6.0. This means that the potential reading is still constant by changing pH. This interval contains wide potential stable range than Barati *et al.*[48] which was 4–6.5 and the interval 4.5–7.7 is case of Abu-Shawish *et al.*[50] Due to base precipitation (un protonated species) at high pH levels, the mV reading decreases and lower readings of EMF were obtained. Competitive protons at lower pH caused an increase in the potential values. In addition, at lower pH, partial protonation has an impact on the ionophore's capacity to bond Cr(III) ions.[51] To provide a potentiometric response, the polar functional groups can combine with metal ions to form complexes in competition with the ionophores.

According to Heidari and Masrournia,[52] changes at elevated pH levels are caused by the development of soluble or insoluble chromium hydroxyl complexes, whereas changes at lower pH ranges are caused by protonation of the ionophore's donor atoms.

3.9. Lifetime

The lifetime of the paste of the proposed electrode was performed by calibration method periodical with standard solution of Cr(III) and calculating the response slope (studying of time factor against Nernstian slope). From the ESI† Fig. (S1), the measurements were done every three days over 70 days, so they gave more accurate results than weekly measurements. Also, it explained that the lifetime of paste was 60 days with no changes in the Nernstian slope.

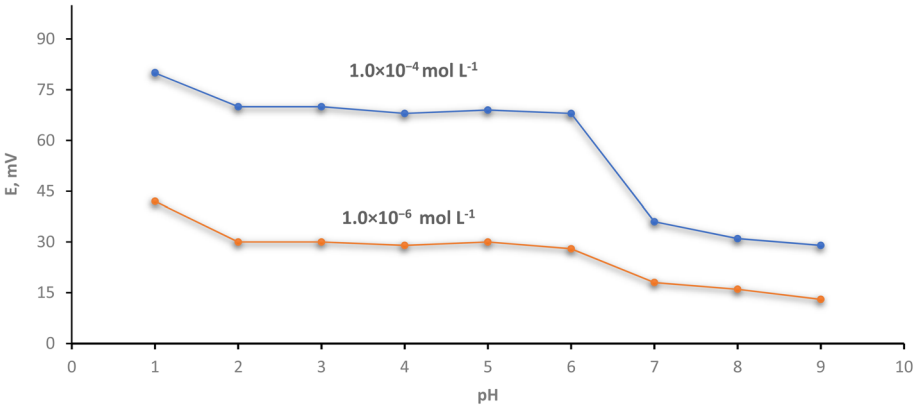

Fig. 5 Validity of pH on the implementation of the investigated electrode.

4. Selectivity coefficients

As shown in Table (1) and ESI† Fig. (S2), the effects of different inorganic cations and sugars on the performance of the electrodes were studied. The selectivity of an electrode is determined not only by the ion mobility, strength of association between the ion and the carrier in the electrode surface, variations in ionic size and permeabilities *etc.*, but also by the ionic strength and the ion concentration ratio factors. There are many methods which used for measuring the selectivity coefficients for the electrode ($K_{A,B}$) as fixed interference method, separate solution method, matched potential method ….*etc.*

First, separate solution method (SSM) in which the potential of the primary ion and interfering ion is measured separately with respect to the activity of the interference (a_B) and the primary ion (a_A) is the same ($a_A = a_B$).[2,12,16] It depends on the Nicolskii–Eisenman equation.

$$\log K_{(A,B)}^{pot} = ((E_2 - E_1)/S) + \log (a_A/(a_B)^{(Z_A/Z_B)})$$

where E_1 is the potential measure of Cr(III) solution and E_2 is the potential of the interfering compound (B). Z_1 and Z_2 are the charges of Cr(III) and interfering species (B) and S is the slope of the electrode calibration graph.

Second, fixed interfering method (FIM) involved a fixed constant activity of the interfering ion a_B, and titration with varying activity of the primary ion. The selectivity coefficient is calculated from the following equation:[2,53]

$$K_{AB} = (a_A/(a_B)^{Z_A/Z_B})$$

where a_A is the activity of the primary ion (Cr(III)) at the lower detection limit in the presence of interfering ion and Z_A and Z_B are the charge of ions (Z_A not equal Z_B). The values of potential were plotted against the concentration of interfering ion.

Table 1 Selectivity coefficient values for MCPE

Interfering compound	$K_{D,B}^{pot}$			
	SSM	FIM	FPM	MPM
Mn^{2+}	9.62×10^{-3}	2.20×10^{-3}	4.20×10^{-3}	—
Ni^{2+}	7.74×10^{-3}	4.42×10^{-3}	7.72×10^{-3}	—
Na^{+}	1.09×10^{-2}	0.51×10^{-2}	0.38×10^{-2}	—
Cu^{2+}	1.93×10^{-3}	2.23×10^{-3}	1.95×10^{-3}	—
Co^{2+}	9.65×10^{-4}	4.41×10^{-3}	1.48×10^{-3}	—
Ba^{2+}	4.34×10^{-3}	1.77×10^{-3}	2.72×10^{-3}	—
Pb^{2+}	2.46×10^{-2}	2.65×10^{-2}	4.20×10^{-2}	—
Ag^{+}	6.87×10^{-3}	7.11×10^{-3}	8.03×10^{-3}	—
Mg^{2+}	5.93×10^{-3}	6.56×10^{-3}	4.66×10^{-3}	—
Ca^{2+}	4.65×10^{-2}	8.09×10^{-3}	9.71×10^{-2}	—
Fe^{3+}	7.03×10^{-3}	9.05×10^{-3}	5.77×10^{-3}	—
Al^{3+}	5.12×10^{-3}	7.54×10^{-3}	8.15×10^{-3}	—
Zn^{2+}	3.45×10^{-3}	4.51×10^{-3}	1.95×10^{-3}	—
Ascorbic acid	1.96×10^{-2}	—	—	—
Fructose	—	—	—	4.95×10^{-2}
Maltose	—	—	—	1.39×10^{-2}
Sucrose	—	—	—	4.34×10^{-2}
Starch	—	—	—	1.09×10^{-2}
Lactose	—	—	—	4.36×10^{-3}

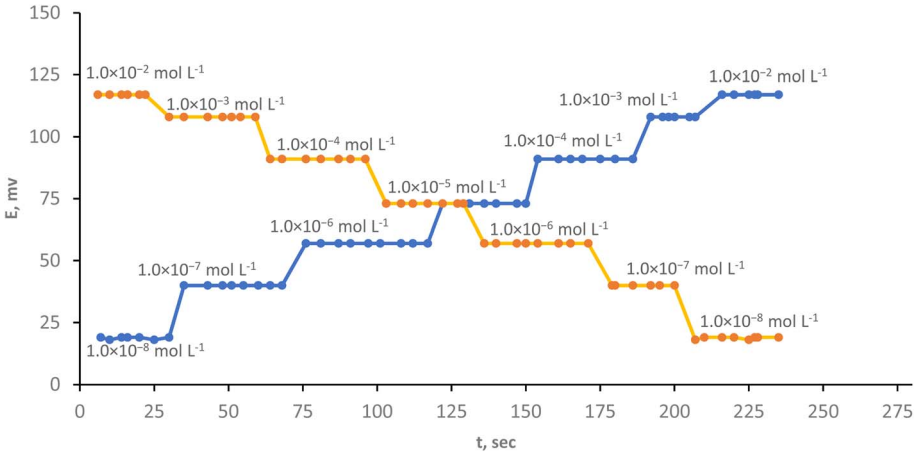

Fig. 6 Effect of response time on the electrode performance.

Third, in fixed primary method (FPM), the values of potential were plotted against the concentration of the interfering ion where the activity of the primary ion is constant.[54] Finally, matched potential method (MPM) is unique because it doesn't depend on the Nicolskii–Eisenman equation like the other methods. Also, it neglects the effect of charges and the Nernstian response of both the primary and interfering ions. So, it is suitable for neutral species and sugars like lactose, starch and fructose and not suitable for charged species like Fe(III), Na(I), Pb(II) and others. Here, the potentiometric selectivity coefficient $K_{A,B}$ is defined as the activity ratio of primary and interfering ions that give the same potential change under identical conditions. At first, a known activity ($a_{A'}$) of the primary ion solution is added into a reference solution that contains a fixed activity (a_A) of primary ions, and the corresponding potential change (ΔE) is recorded. Next, a solution of an interfering ion is added to the reference solution until the same potential change (ΔE) is recorded. The change in potential produced at the constant background of the primary ion must be the same in both cases.[2,18] $K_{A,B} = (a_{A'} - a_A)/a_B$

From Table (1), it is clear that high selectivity coefficient values in the state of sugars, ascorbic acid and other metal ions is observed. This is due to the polarity, atomic size, and lipophilic nature of their molecules in respect to Cr(III) solution. Also, it explains usage of diverse metal ions with varying atomic sizes and oxidation values were employed as interfering entities. It is noted that values of selectivity coefficient are smaller than 1.0 indicating that the sensor is responding more to primary ion than to interfering ions and in such cases the sensor is said to be more selective to primary ion over interfering ions.[2,12,16,52]

4.1. Effect of temperature

The temperature's impact on the potentiometric electrode's performance was assessed from 10 to 60 °C, and the isothermal coefficient ($dE°/dT$) will be adjusted for each electrode in accordance with the giving equation:[19] $E^\circ_{cell} = E^\circ_{cell}(25) + (dE^\circ/dT)(t - 25)$.

In the temperature range of 10 to 60 °C, it is noticeable that the electrode provided a satisfactory Nernstian reaction. The isothermal coefficient is expressed by the slope of the resulting straight line, which was established to be 0.743×10^{-3} V per °C. The extraordinarily high thermal stability of the electrode was evidenced by the extremely minimal value of the isothermal coefficient. This shows that the tested electrode may be employed up to 60 °C without significantly deviating from Nernstian behavior with reliable results for the measurement of Cr(III) ions.[16]

Table 2 Evaluation of examined CPE's intra- and inter-day accuracy and precision; for $n = 5$

Form	[Cr(III)]	Intra-day			Inter-day		
Type of sample	Taken mg mL^{-1}	Found mg mL^{-1}	Recovery (%)±SD	RSD%	Found mg mL^{-1}	Recovery (%)±SD	RSD%
Pure	0.239	0.233	97.49 ± 0.008	3.43	0.233	97.49 ± 0.007	3.00
Water	0.239	0.235	98.33 ± 0.007	2.30	0.234	97.90 ± 0.009	3.85
Tea	0.239	0.240	100.4 ± 0.009	3.75	0.229	95.82 ± 0.012	3.34
Cheese	0.239	0.241	100.8 ± 0.002	0.83	0.237	99.16 ± 0.004	1.69
Milk	0.239	0.238	99.58 ± 0.003	1.26	0.238	99.58 ± 0.003	1.26
Honey	0.239	0.240	100.4 ± 0.009	3.75	0.237	99.16 ± 0.001	0.38
Coffee	0.239	0.237	99.16 ± 0.001	0.42	0.236	98.74 ± 0.004	1.69
Cosmetic	0.239	0.238	99.58 ± 0.002	0.84	0.235	98.33 ± 0.002	0.85

Table 3 Comparison of ICP-MS and studied CPE for the detection of pure Cr(III) and other spiked authentic samples[a]

		[Cr(III)]			
Type of method	Type of Sample	Taken mg mL^{-1}	Found mg mL^{-1}	Recovery (%)±SD	RSD%
Potentiometry	Pure[b]	0.0260	0.0259	99.62 ± 0.0004	1.54
	Water[c]		0.0246	94.62 ± 0.0008	3.25
	Tea		0.0256	98.46 ± 0.0006	2.69
	Cheese		0.0251	96.54 ± 0.0005	2.31
	Milk		0.0248	95.83 ± 0.0009	3.77
	Honey		0.0257	98.85 ± 0.0010	4.14
	Coffee		0.0259	99.62 ± 0.0009	3.43
	Cosmetic		0.0258	99.23 ± 0.0009	3.56
ICP-MS	Pure[b]	0.0260	0.0245	94.23 ± 0.0006	2.44
	Water[c]		0.0249	95.77 ± 0.0011	4.01
	Tea		0.0255	98.08 ± 0.0003	1.18
	Cheese		0.0254	97.69 ± 0.0093	3.54
	Milk		0.0255	98.08 ± 0.0002	1.96
	Honey		0.0248	95.38 ± 0.0012	4.03
	Coffee		0.0251	96.50 ± 0.0007	2.78
	Cosmetic		0.0257	98.85 ± 0.0004	1.56

[a] At $n = 5$, 95% confidence level, F-test (tabulated) = 5.190, t-test (tabulated) = 2.571 F-test (experimental) = 0.01–4.80, t-test (experimental) = 0.02–2.40. [b] Pure: Cr(III) solution in double distilled water. [c] Water: tap water spiked with known amount of Cr(III) ion.

4.2. Effect of response time

The phrase "response time" refers to the average duration of time it takes for the electrode to balance at a voltage that is within ±1 mV of the final equilibrium value. The time constant of the electrode's response function is substantially bigger, this due to several factors, such as the measurement device's time constant, the rate of ion transfer reaction at the paste–pattern interface, the impedance of the paste's equivalent electric circuit, or the stability of a liquid-junction potential at the reference electrode, directly impact the entire response time.[53] Fig. (6) makes it evident that the electrode has a quick response time of 7 s even when it measured forward (from lower concentration to higher concentration) or backward (from higher concentration to lower concentration). This is owing to the inclusion of the optimum ion pair content and a good solvent moderator. Contrasting to our finding, Shojaei *et al.*[55] reported that the sensor's reaction time for identifying Cr(III) ions is around 10 s and Barati, *et al.* response sensor's time was smaller than 15 s.[48]

Table 4 Comparison between the previously reported sensors and proposed sensor for Cr(III) ion determination

Modifier	Slope (mV $decade^{-1}$)	Detection limit, mol L^{-1}	Linear range, mol L^{-1}	pH range	Response time, s	Lifetime (month)	Interfering ions with $\log k_{Cr(III),J}^{pot} \geq -2$	Ref.
N-(Aceto acetanilide)-1,2-diaminoethane	19.8	5.60×10^{-8}	8.9×10^{-8}–1.0×10^{-1}	2.0–7.0	10	3	No interference	62
N, *N* bis(salicylidene)-*o*-phenylenediaminatechromium(III)	20.1	1.80×10^{-6}	7.5×10^{-6}–1.0×10^{-2}	4.5–7.7	8	Not mentioned	Pb(II), Hg(II) and Al(III)	50
5-Amino-1-phenyl-1H-pyrazole-4-carboxamide	19.6	5.30×10^{-7}	1.0×10^{-6}–1.0×10^{-1}	3.2–6.3	10	2	Ca(II)	61
1-[(2-Hydroxy ethyl) amino]-4-methyl-9H-thioxanthen-9-one	20.51	1.60×10^{-7}	3.2×10^{-7}–1.0×10^{-1}	4.8–6.3	10	Not mentioned	Co(II), Sr(II), Mg(II) Ba(II) and K(I)	60
p-(4-Acetanilidazo) calix[4] arene	19.8	Not mentioned	9.8×10^{-7}–1.0×10^{-1}	2.8–5.7	10	3	Fe(III)	63
1-(2-(1H-Imidazole-1-yl)-1-(4-methoxyphenyl) ethylidene)-2-phenyl hydrazine	19.6	6.80×10^{-8}	8.4×10^{-8}–1.0×10^{-2}	3.3–5.9	10	2	Al(III) and Ag(I)	59
N-[4-(Dimethylamino)benzylidene]-6-nitro-1,3-benzothiazol-2-amine	20	2.0×10^{-7}	4.0×10^{-6}–1.0×10^{-1}	2.8–5.1	15	5	No interference	2
Nano chromium complex	18.8	1.00×10^{-8}	1.0×10^{-8}–1.0×10^{-2}	2.0–6.0	8	3	Fe(III)	64
t-ZrO_2 nanoparticles	19.5	1.00×10^{-8}	1.0×10^{-8}–1.0×10^{-2}	2.0–6.0	8	2	No interference	This study

4.3. Method validation

Considering the ideal experimental circumstances, the analytical approach was established in accordance with the standards of the International Conference for Harmonization (ICH): accuracy, specificity, precision, limit of detection (LOD), linearity and limit of quantification (LOQ) were realized for standard Cr(III) ion solution.[7,56] LOD stands for lowest detectable dose of the examined substance in the sample, although it might not be evaluated with a tolerable level of uncertainty. When the concentration varies slightly without causing any discernible change in the response, it was the concentration of detected ions at the junction of the extrapolated linear portion of the calibration curve reflecting the normal slope of the electrode and the horizontal line denoting the voltage when the concentration is so low that small change in concentration don't produce any detectable change in the response of electrode.[4] The LOD was 1.0×10^{-8} mol L^{-1}, which is better than the value published in Barati *et al.*[48] which was 3.1×10^{-7} mol L^{-1} in the concentration from 5.0×10^{-7} to 1.0×10^{-3} mol L^{-1}. The data revealed that the sensor has a high sensitivity and can be used to detect low levels of Cr(III) ion concentration, as revealed in ESI† Table (S2).

LOQ is The smallest amount of a material that may be precisely and correctly quantified in a sample matrix.[12] According to ESI† Table (S2) and Fig. (S3), it was discovered that the LOQ was 3.33×10^{-8} mol L^{-1}, it is indicated that this electrode has more sensitive measurements towards the determination of Cr(III) (LOQ = 10 LOD/3).

Accuracy is a crucial requirement for analytical techniques and refers to the extent to which the resulting value is close to the true or considered as the reference value. Table 2 shows that the high percentage recovery statistics ensure the method's high accuracy. The extent to which outcomes agree with one another is a measure of precision. The replicated analyses' standard or relative standard deviations are generally employed to express it. Using pure Cr(III) solution and some real samples, inter- and intra-day precisions were considered across five replicates. The minimal relative standard deviation values reflect the method's outstanding repeatability and reproducibility (Table (2)).

The degree to which the calibration plot of electrochemical potential *vs.* concentration resembles a straight line is known as linearity. Using a standard Cr(III) solution, the standard calibration curve was generated. As indicated in ESI †Table (S2) and Fig. (S3), a linear relation between negative log[Cr(III)] and potential (mV) was established.[57,58] The linear range for the investigated CPE was 1.0×10^{-8} – 1.0×10^{-2} mol L^{-1}.

The process of determining specificity involved screening for any interference from typical excipients. The outcome of the suggested method was found to be unaffected by these components, ESI† Fig. (S2).

4.4. Applications

Utilizing the potentiometric calibration approach, the designed sensor was employed to recognize the chromic ion in a variety of samples, including tea, coffee, milk, cheese, honey, and cosmetics. Inductively coupled plasma mass spectrometry (ICP-MS) findings and potentiometric calibration method results were compared,[19–21] and the results of this comparison were presented in Table (3). In regards of recovery and relative standard deviation, the analysis of the Cr(III) ion in both pure solution and spiked samples achieved encourageable findings, indicating the superior accuracy and precision of the suggested electrode. These results also compared with results of ICP technique. It is found that the values of F-test ranged from 0.01 to 4.80. On the other hand, the values of *t*-test were ranged from 0.02 to 2.40. According to this comparison, it showed no noticeable changes between the two approaches, hence highlighting its benefits. It is clear from these data that the calculated *F*- and *t*-test values are lower than the tabulated values at 95% confidence level supporting the nonsignificant difference between the reported potentiometric method and ICP method.

4.5. Comparative study

It would be acceptable to state that this sensor displayed increased selectivity and sensitivity for the selective detection of Cr(III) ions in comparison to the latterly described potentiometric sensors[2,50,59–64] (Table (4)). This could be explained by the exceptional characteristics of the used nano t-ZrO_2 ionophore, such as its surface area, porous structure, mechanical, and conductivity capabilities. It was clear from Table (4) that the proposed sensor has LOD value, linear concentration range and pH range comparable or sometimes better than the reported ones. The potentiometry approach additionally offers advantages including simplicity, low cost, the lack of sample fabrication, and quick response. CPEs are reliable, chemically inert, affordable, renewable, and stable.

5. Conclusion

Pure nano-t-ZrO_2 was synthesized utilizing a modified co-precipitation method with a 14% MgO stabilizer, and it was then fully characterized *via* different characterization methods. The selectivity and sensitivity toward the Cr(III) ion improved after the carbon paste composition was properly optimized. The redesigned electrode had favorable Nernstian slope, a low detection limit, a high recovery percentage, low standard deviation and relative standard deviation values. This straightforward, affordable, and renewable chromic ion sensor might be used in various authentic samples. In light of this, the newly developed sensor might be a useful addition to the list of Cr(III) sensors already in use.

Conflicts of interest

The authors affirm that they do not have any conflicting interests.

References

1 J. Emsley, *Nature's building blocks: an AZ guide to the elements*, Oxford University Press, 2011.

2 T. A. Ali, A. L. Saber, G. G. Mohamed and T. M. Bawazeer, Determination of Cr (III) ions in different water samples using chromium (III)-sensor based on N-[4-(dimethylamino) benzylidene]-6-nitro-1, 3-benzothiazol-2-amine, *Int. J. Electrochem. Sci.*, 2014, **9**(9), 4932–4943.

3 X. R. Xu, H. B. Li, J. D. Gu and X. Y. Li, Kinetics of the reduction of chromium (VI) by vitamin C, *Environ. Toxicol. Chem.*, 2005, **24**(6), 1310–1314.

4 O. A. Fouad, A. E. Ali, G. G. Mohamed and N. F. Mahmoud, Ultrasonic aided synthesis of a novel mesoporous cobalt-based metal-organic framework and its application in Cr (III) ion determination in centrum multivitamin and real water samples, *Microchem. J.*, 2022, **175**, 107228.

5 J. Sahu, J. Acharya and B. Meikap, Response surface modeling and optimization of chromium (VI) removal from aqueous solution using Tamarind wood activated carbon in batch process, *J. Hazard. Mater.*, 2009, **172**(2–3), 818–825.

6 A. A. Belay, Impacts of chromium from tannery effluent and evaluation of alternative treatment options, *J. Environ. Prot.*, 2010, **1**(01), 53.

7 A. Wiryawan, R. Retnowati, P. Burhan and S. Syekhfani, Method of analysis for determination of the chromium (Cr) species in water samples by spectrophotometry with diphenylcarbazide, *J. Environ. Eng. Sustainable Technol.*, 2018, **5**(1), 37–46.

8 N. Fabregat-Cabello, P. Rodriguez-Gonzalez, A. Castillo, J. Malherbe, A. F. Roig-Navarro, S. E. Long and J. I. G. Alonso, Fast and accurate procedure for the determination of Cr (VI) in solid samples by isotope dilution mass spectrometry, *Environ. Sci. Technol.*, 2012, **46**(22), 12542–12549.

9 Z. Sun and P. Liang, Determination of Cr (III) and total chromium in water samples by cloud point extraction and flame atomic absorption spectrometry, *Microchim. Acta*, 2008, **162**(1), 121–125.

10 B. Umesh, R. M. Rajendran and M. T. Manoharan, Method for the determination of chromium in feed matrix by HPLC, *Poult. Sci.*, 2015, **94**(11), 2805–2815.

11 P. Riss, E. Connor, and A. Ryan, *Determination of Low Levels of Chromium in Biological Samples by ICP-MS Using Hydrogen as a Reaction Gas*, 2017.

12 N. F. Mahmoud, O. A. Fouad, A. E. Ali and G. G. Mohamed, Potentiometric determination of the Al (III) ion in polluted water and pharmaceutical samples by a novel mesoporous copper metal–organic framework-modified carbon paste electrode, *Ind. Eng. Chem. Res.*, 2021, **60**(6), 2374–2387.

13 G. Manasa, A. K. Bhakta, Z. Mekhalif and R. J. Mascarenhas, Voltammetric study and rapid quantification of resorcinol in hair dye and biological samples using ultrasensitive maghemite/MWCNT modified carbon paste electrode, *Electroanalysis*, 2019, **31**(7), 1363–1372.

14 N. Shetti and D. Nayak, Electrochemical detection of chlorpheniramine maleate in the presence of an anionic surfactant and its analytical applications, *Can. J. Chem.*, 2017, **95**(5), 553–559.

15 M. R. Mohammad, G. G. Mohamed, T. A. Ali, E. Y. Farag and M. E. B. Mohammad, Electrochemical performance of screen printed sensors for potentiometric determination of anticholinergic oxybutynine hydrochloride in pharmaceutical formulations and biological fluids, *Egypt. J. Chem.*, 2020, **63**(5), 1799–1809.

16 T. A. Ali, A. A. Abd-Elaal and G. G. Mohamed, Screen printed ion selective electrodes based on self-assembled thiol surfactant-gold-nanoparticles for determination of Cu (II) in different water samples, *Microchem. J.*, 2021, **160**, 105693.

17 N. P. Shetti, S. J. Malode, D. S. Nayak, C. V. Reddy and K. R. Reddy, Novel biosensor for efficient electrochemical detection of methdilazine using carbon nanotubes-modified electrodes, *Mater. Res. Express*, 2019, **6**(11), 116308.

18 N. P. Shetti, S. J. Malode, D. S. Nayak and K. R. Reddy, Novel heterostructured Ru-doped TiO2/CNTs hybrids with enhanced electrochemical sensing performance for Cetirizine, *Mater. Res. Express*, 2019, **6**(11), 115085.

19 N. P. Shetti, D. S. Nayak, K. R. Reddy and T. M. Aminabhvi, Graphene–clay-based hybrid nanostructures for electrochemical sensors and biosensors, in *Graphene-based electrochemical sensors for biomolecules*, Elsevier, 2019. pp. 235–274.

20 S. D. Bukkitgar, N. P. Shetti and R. M. Kulkarni, Construction of nanoparticles composite sensor for atorvastatin and its determination in pharmaceutical and urine samples, *Sens. Actuators, B*, 2018, **255**, 1462–1470.

21 N. P. Shetti, S. J. Malode, D. Ilager, K. Raghava Reddy, S. S. Shukla and T. M. Aminabhavi, A novel electrochemical sensor for detection of molinate using ZnO nanoparticles loaded carbon electrode, *Electroanalysis*, 2019, **31**(6), 1040–1049.

22 G. Manasa, R. J. Mascarenhas and B. M. Basavaraja, Sensitively-selective determination of Propyl Paraben preservative based on synergistic effects of polyaniline-zinc-oxide nano-composite incorporated into graphite paste electrode, *Colloids Surf., B*, 2019, **184**, 110529.

23 S. Kaul, N. Srivastava, V. Rana and N. Kaushik, Zirconia Crowns–The Esthetic Triumph of Pediatric Dentistry: A Literature Review, *Int. J. All Res. Educ. Sci. Methods*, 2022, **10**, 758–763.

24 K. Shanmugam and R. Sahadevan, *Bioceramics-an introductory overview.* Fundamental biomaterials: ceramics, 2018, pp. 1–46.

25 G. Chen, Y. Ling, Q. Li, H. Zheng, K. Li, Q. Jiang, L. Gao, M. Omran, J. Peng and J. Chen, Stability properties and structural characteristics of CaO-partially stabilized zirconia ceramics synthesized from fused ZrO2 by microwave sintering, *Ceram. Int.*, 2020, **46**(10), 16842–16848.

26 G. Chen, Q. Li, Y. Ling, H. Zheng, J. Chen, Q. Jiang, K. Li, J. Peng, M. Omran and L. Gao, Phase stability and microstructure morphology of microwave-sintered magnesia-partially stabilised zirconia, *Ceram. Int.*, 2021, **47**(3), 4076–4082.

27 J. CESARANO III, I. A. Aksay and A. Bleier, Stability of aqueous α-Al2O3 suspensions with poly (methacrylic acid) polyelectrolyte, *J. Am. Ceram. Soc.*, 1988, **71**(4), 250–255.

28 Q. Li, Y. Ling, H. Zheng, G. Chen, J. Chen, S. Koppala, Q. Jiang, K. Li, M. Omran and L. Gao, Phase microstructure and morphology evolution of MgO-PSZ ceramics during the microwave sintering process, *Ceram. Int.*, 2021, **47**(11), 15849–15858.
29 R. C. Garvie and P. S. Nicholson, Structure and thermomechanical properties of partially stabilized zirconia in the CaO-ZrO2 system, *J. Am. Ceram. Soc.*, 1972, **55**(3), 152–157.
30 S. Fabris, A. T. Paxton and M. W. Finnis, A stabilization mechanism of zirconia based on oxygen vacancies only, *Acta Mater.*, 2002, **50**(20), 5171–5178.
31 M. Yan, Y. Li, G. Yin, S. Tong and J. Chen, Synthesis and characterization of a MgO-MgAl2O4-ZrO2 composite with a continuous network microstructure, *Ceram. Int.*, 2017, **43**(8), 5914–5919.
32 K. Li, J. Chen, J. Peng, S. Koppala, M. Omran and G. Chen, One-step preparation of CaO-doped partially stabilized zirconia from fused zirconia, *Ceram. Int.*, 2020, **46**(5), 6484–6490.
33 C.-W. Kuo, Y.-H. Shen, F.-L. Yen, H.-Z. Cheng, I.-M. Hung, S.-B. Wen, M.-C. Wang and M. Stack, Phase transformation behavior of 3 mol% yttria partially-stabilized ZrO2 (3Y–PSZ) precursor powder by an isothermal method, *Ceram. Int.*, 2014, **40**(2), 3243–3251.
34 E. Tani, M. Yoshimura and S. SOmiya, Revised phase diagram of the system ZrO2-CeO2 below 1400 °C, *J. Am. Ceram. Soc.*, 1983, **66**(7), 506–510.
35 H. Wang, M. Wang, W. Zhang, N. Zhao, W. Wei and Y. Sun, Synthesis of dimethyl carbonate from propylene carbonate and methanol using CaO–ZrO2 solid solutions as highly stable catalysts, *Catal. Today*, 2006, **115**(1–4), 107–110.
36 H. Wang, M. Wang, N. Zhao, W. Wei and Y. Sun, CaO–ZrO2 solid solution: a highly stable catalyst for the synthesis of dimethyl carbonate from propylene carbonate and methanol, *Catal. Lett.*, 2005, **105**(3), 253–257.
37 A. Sharma and B. Ahn, Effect of MgO Addition on the Monoclinic to Tetragonal Transition of ZrO2 Fabricated by High Energy Ball Milling, *Korean J. Met. Mater.*, 2018, **56**(10), 718–726.
38 R. C. Garvie, R. Hannink and R. Pascoe, Ceramic steel?, *Nature*, 1975, **258**(5537), 703–704.
39 O. A. Fouad, M. M. Wahsh, G. G. Mohamed and M. M. El Desssouky, Fabrication and characterization of macroporous alumina-nano tetragonal zirconia-nano spinel ceramic composites, *Mater. Chem. Phys.*, 2023, **301**, 127617.
40 R. Al Sidawi, G. Ghambashidze, T. Urushadze and A. Ploeger, Heavy metal levels in milk and cheese produced in the Kvemo Kartli region, Georgia, *Foods*, 2021, **10**(9), 2234.
41 A. Gebrekidan and A. A. Desta, Assessment on the levels of selected essential and non-essential metals in sesame seeds (Sesamum indicum L.) collected from Sheraro town, Northwest Tigray, Ethiopia, *Bull. Chem. Soc. Ethiop.*, 2019, **33**(2), 191–202.
42 A. d. S. Sabrina, Q. M. Fabrcia, R. R. Marcelo, R. P. Flavia, M. X. d. C. Andre, R. d. O. R. Katia and G. P. Frederico, Determination of heavy metals in the roasted and ground coffee beans and brew, *Afr. J. Agric. Res.*, 2017, **12**(4), 221–228.
43 N. Alsaffar and H. Hussein, Determination of heavy metals in some cosmetics available in locally markets, *IOSR J. Environ. Sci., Toxicol. Food Technol.*, 2014, **8**(1), 9–12.
44 M. A. Nkansah, M. Shamsu-Deen and F. Opoku, Phytocompounds, heavy metal and mineral contents in honey samples from selected markets in the Kumasi metropolis, *Emerg. Sci. J.*, 2018, **2**(5), 287–294.
45 O. A. Fouad, M. M. Wahsh, G. G. Mohamed, M. M. El Desssouky and M. R. Mostafa, Fabrication and characterization of mullite nano-ceramic materials for use in carbon paste ion selective electrode to estimate carcinogenic Cd (II) ion in real and human samples, *Microchem. J.*, 2023, **190**, 108623.
46 A. Delvallée, M. Oulalite, L. Crouzier, S. Ducourtieux, N. Lambeng, W. Amor, N. B. Ghomrasni, N. Feltin, A. Viot and C. Jamet, Correlation of AFM/SEM/EDS Images to Discriminate Several Nanoparticle Populations Mixed in Cosmetics, *Microsc. Today*, 2021, **29**(3), 46–51.
47 M. Wahsh, T. Mansour, A. Othman and I. Bakr, Recycling bagasse and rice hulls ash as a pore-forming agent in the fabrication of cordierite-spinel porous ceramics, *Int. J. Appl. Ceram. Technol.*, 2022, **19**, 2664–2674.
48 Z. Barati, M. Masrournia, Z. Es' haghi, M. Jahani and J. Ebrahimi, Selective determination of Cr (III) by modified carbon nanotube paste electrode: a potentiometric study, *J. Chem. Technol. Biotechnol.*, 2022, **97**(5), 1234–1239.
49 M. A. d. l. A. A. Pérez, L. P. Marin, J. C. Quintana and M. Yazdani-Pedram, Influence of different plasticizers on the response of chemical sensors based on polymeric membranes for nitrate ion determination, *Sens. Actuators, B*, 2003, **89**(3), 262–268.
50 H. Abu-Shawish, S. Saadeh, K. Hartani and H. Dalloul, A comparative study of chromium (III) ion-selective electrodes based on N, N-bis (salicylidene)-o-phenylenediaminatechromium (III), *J. Iran. Chem. Soc.*, 2009, **6**(4), 729–737.
51 M. Zayed, A. A. Abbas, W. H. Mahmoud, A. E. Ali and G. G. Mohamed, Development and surface characterization of a bis (aminotriazoles) derivative based renewable carbon paste electrode for selective potentiometric determination of Cr (III) ion in real water samples, *Microchem. J.*, 2020, **159**, 105478.
52 Z. Heidari and M. Masrournia, A novel modified carbon paste electrode for the determination of chromium (III) in water, *J. Anal. Chem.*, 2018, **73**(8), 824–831.
53 Y. Umezawa, K. Umezawa and H. Sato, Selectivity coefficients for ion-selective electrodes: recommended methods for reporting KA, Bpot values (Technical Report), *Pure Appl. Chem.*, 1995, **67**(3), 507–518.
54 M. Raulf, N. Buschmann and D. Sommer, Determination of anionic surfactants in lubrication fluids, *Fresenius' J. Anal. Chem.*, 1995, **351**(6), 526–529.
55 E. Shojaei, M. Masrournia, A. Beyramabadi and H. Behmadi, Design and fabrication of carbon paste electrode for determination of Cr(III) ion in real water samples using

a new synthesis Schiff base as selective ionophore, *Eurasian Chem. Commun.*, 2020, **2**(7), 750–759.

56 Y. Ishii, M. Iijima, T. Umemura, A. Nishikawa, Y. Iwasaki, R. Ito, K. Saito, M. Hirose and H. Nakazawa, Determination of nitrotyrosine and tyrosine by high-performance liquid chromatography with tandem mass spectrometry and immunohistochemical analysis in livers of mice administered acetaminophen, *J. Pharm. Biomed. Anal.*, 2006, **41**(4), 1325–1331.

57 P. Pradhan, R. J. Mascarenhas, T. Thomas, I. N. Namboothiri, O. J. D'Souza and Z. Mekhalif, Electropolymerization of bromothymol blue on carbon paste electrode bulk modified with oxidized multiwall carbon nanotubes and its application in amperometric sensing of epinephrine in pharmaceutical and biological samples, *J. Electroanal. Chem.*, 2014, **732**, 30–37.

58 H. Yi, D. Zheng, C. Hu and S. Hu, Functionalized multiwalled carbon nanotubes through in situ electropolymerization of brilliant cresyl blue for determination of epinephrine, *Electroanalysis*, 2008, **20**(10), 1143–1146.

59 A. Abbaspour, M. Refahi, A. Khalafi-Nezhad, N. S. Rad and S. Behrouz, Carbon composite–PVC based membrane coated platinum electrode for chromium determination, *J. Hazard. Mater.*, 2010, **184**(1–3), 20–25.

60 M. Ghaedi, A. Shokrollahi, A. Salimibeni, S. Noshadi and S. Joybar, Preparation of a new chromium (III) selective electrode based on 1-[(2-hydroxy ethyl) amino]-4-methyl-9H-thioxanthen-9-one as a neutral carrier, *J. Hazard. Mater.*, 2010, **178**(1–3), 157–163.

61 H. A. Zamani, G. Rajabzadeh, M. Masrornia, A. Dejbord, M. R. Ganjali and N. Seifi, Determination of Cr3+ ions in biological and environmental samples by a chromium (III) membrane sensor based on 5-amino-1-phenyl-1H-pyrazole-4-carboxamide, *Desalination*, 2009, **249**(2), 560–565.

62 A. K. Singh, V. Gupta and B. Gupta, Chromium (III) selective membrane sensors based on Schiff bases as chelating ionophores, *Anal. Chim. Acta*, 2007, **585**(1), 171–178.

63 P. Kumar and Y.-B. Shim, Chromium (III)-selective electrode using p-(4-acetanilidazo) calix [4] arene as an ionophore in PVC matrix, *Bull. Korean Chem. Soc.*, 2008, **29**(12), 2471–2476.

64 T. A. Ali and G. G. Mohamed, Development of chromium (III) selective potentiometric sensors for its determination in petroleum water samples using synthesized nano Schiff base complex as an ionophore, *J. AOAC Int.*, 2022, **105**(3), 727–738.